*FRENCH-UKRAINIAN JOURNAL OF CHEMISTRY (**2026**, VOLUME **14**, ISSUE **01**)*

Temperature Regimes in Layered Interaction of Ferrosilicon Alloy with Water during Hydrogen Production

Mykola Zipunnikov[a*], Svetlana Bukhkalo[b]

[a]*A.M. Pidhorny Institute of Power Machines and Systems of NASU (IPMash NAS of Ukraine), 2/10, Komunalnykiv str., 61046, Kharkiv, Ukraine*

[b]*Ukrainian state university of science and technologies, 2, Lazaryan str., 49010, Dnipro, Ukraine*

zipunnikov_n@ukr.net

Keywords*: ferrosilicon alloy, hydrogen generation, temperature, aluminum, reactor.*

The article investigates the temperature regimes of the reaction surface of the hydroxide layer formed on the surface of ferrosilicon alloy (FS90Ba4) during layer-by-layer interaction with aqueous sodium hydroxide solution in a glass reactor. The interaction of FS90Ba4 alloy samples with aqueous NaOH solution was further studied in a hydrogen reactor operating under isochoric conditions ($V = 1.13\times10^{-3}$ m³). Temperature–time profiles were analyzed, and the motion and fluid flow velocity around of spherical FS90Ba4 alloy particles during their interaction with aqueous sodium hydroxide solution in the hydrogen reactor were determined.

Introduction

The expansion of hydrogen application areas is linked to the qualitative changes currently taking place in the chemical, machine-building, metallurgical, and energy sectors.

Recent studies have addressed hydrogen production technologies, with a focus on photoelectrochemical methods and renewable energy-based technologies [1-7]. The papers [8-14] examines the operating principles of water electrolysis cells, maps out technological innovation gaps, and explores development opportunities in proton exchange membranes and solid oxide electrolysis.

Hydrogen generation technologies based on energy-accumulating substances have been developed for decades.

In the development of hydrogen generation technologies, reactions involving aluminum or silicon with caustic soda solutions, as well as calcium hydride with water, are used to produce this gas. The silicon-based method of hydrogen generation from water is employed at autonomous facilities, particularly at meteorological stations and in aerostatic organizations. However, this process requires substantial consumption of reagents and caustic soda [15-34]. Simplicity of operation and sufficiently high efficiency are the main advantages of hydrogen-generating systems that use the silicon method. The implementation of more economical hydrogen generation methods and equipment is limited because the general theory of alloy-water interaction is still in an early stage of development. To date, the thermodynamics, kinetics, and heat and mass

transfer have been studied mainly for the interaction of caustic soda solutions with various standard aluminum powders, as well as with aluminum activated by indium, gallium, and tin.

Regarding silicon alloys, experiments have been carried out with ferrosilicon FS 75 and ferrosilicon–aluminum alloys (FSA) obtained by alloying pure components [16, 17-22], as well as with FSA produced from the inorganic fraction of low-calorie coal and with amorphous-crystalline FSA [22, 24-26].

The study [35] found that the gravimetric storage capacity for hydrogen in ferrosilicon 75 is therefore maintained at only 3.5% rather than the 10.5% ideally expected for a material containing 75% silicon. In light of these results, ferrosilicon 75 does not appear to be a good candidate for hydrogen production in portable applications.

In this context, an important and timely challenge is the optimization of technologies for hydrogen production from water, as well as the establishment of design standards for hydrogen generators, based on experimental and theoretical studies of the mechanism of heterogeneous hydrolysis reactions of ferrosilicon with alkaline-earth metal additives.

Purposes and research tasking

Determination of the temperature regimes of the reaction surface of the hydroxide layer formed on the surface of a ferrosilicon alloy (FS90Ba4) under conditions of layer-by-layer interaction with an aqueous sodium hydroxide solution in a glass reactor.

To analyze the temperature–time profiles and determine the motion and wetting rates of spherical ferrosilicon particles during their interaction with aqueous NaOH solution in a hydrogen reactor.

Experimental methods

The method of hydrogen generation when using the silicon based-alloys is described by the equation [36]

$$Si + 2NaOH + H_2O \leftrightarrow Na_2SiO_3 + 2H_2\uparrow.$$

According to the stoichiometry, it is necessary to take 80 g of the sodium hydroxide for every 28 g of the silicon. But the practice of hydrogen generation, especially in the high pressure gas generators, has shown that the amount of sodium hydroxide can be much less, since the hydrolysis of the sodium silicates is according to the equation

$$2Na_2O{\cdot}SiO_2 + H_2O \leftrightarrow 2NaOH + Na_2O{\cdot}2SiO_2.$$

As a result, the free NaOH is liberated and sodium silicate is formed with a module of

n = 2. In the technical practice the sodium silicates are commonly referred to as soluble glass, and their solutions – as the liquid glass. The main characteristic of the soluble glass is the number *n*, which shows how many the silicon molecules SiO_2 is charged per one molecule of the sodium oxide Na_2O. The sodium silicate with n = 2 can be further hydrolyzed with forming the silicates with a larger module. The solution of silicates in water can be in general represented by the formula $Na_2O{\cdot}nSiO_2{\cdot}mH_2O$, where *m* is the number of those water molecules that are included in the silicates.

The number of repeated experiments was at least three, and the deviation of

measurement results in repeated experiments did not exceed 3-4 %. The heat-and-mass transfer experiments were performed in a glass reactor. As a reference material, the activated aluminum alloy AG5O5In5 (mass %: Fe − 5.9, Si − 88.6, Ba − 4.0, Ca − 1.5) [37] was used for comparison. A thermocouple was placed at the center of the cube, whose wall thickness was (8-12)×10^{-3} m. Initially the thermocouple junction was insulated with a cotton layer. A hole for the thermocouple (d_{hole} = 3×10^{-3} m) was then filled with epoxy. The contact between the thermocouple and the cube body was verified with a tester. The temperature at the center of the alloy sample was monitored simultaneously with the temperature of the surrounding environment (reactor). The surface temperature of the sample was measured with a Chromel–Alumel (Type K) thermocouple probe during the reaction conducted in an open vessel. The thermocouple was calibrated using an electric furnace and an ice bath within the operating temperature range (0-150 °C).

Figure 1 shows the temperature changes on the surface of the reacting FS90Ba4 sample and at the sample center during the reaction in the open vessel.

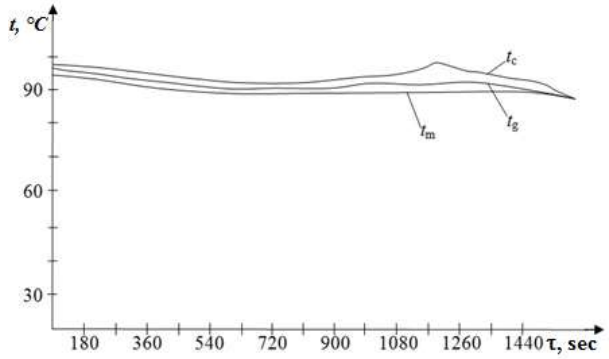

Figure 1. Temperature–time profiles for the reaction of FS90Ba4 alloy with 13.3 % NaOH: t_{start} = 95 °C – initial reaction temperature; t_m − solution temperature; t_c – temperature at the center of the alloy sample; t_g – temperature of the outer surface of the hydroxide layer; m = 4.2·10^{-3} kg.

The temperature of the outer surface of the hydroxide layer at the gas evolution sites (t_g) was found to be 2.3-3.1 °C higher than the average temperature of the reaction solution (t_m), while the temperature at the sample center (t_c) exceeded it by 3.1-5.3 °C.

As the reaction front approaches the thermocouple junction at the sample center, a sharp temperature increase of 7-9 °C is observed under boiling and gas evolution conditions. The temperature difference between the reaction solution and the center of the ferrosilicon alloy sample ranged from 88-97 °C. A large temperature spike occurs at higher temperatures and lasts for 40-50 seconds.

After the temperature spike, the measuring device recorded the average temperature, which was additionally verified using a mercury thermometer. This confirms that the reaction has finished due to the complete destruction of the sample. It should be noted that a well-defined heat-exchange intensity corresponds to the observed temperature spike (t_m–t_c). To calculate

heat transfer from the reacting particle to the surrounding fluid, it is necessary to determine the velocity of the circulating flow. The experiments showed that an FS90Ba4 alloy cube exhibits almost no reaction in hot water at 90 °C, whereas in a 13.3 % NaOH solution at 95 °C the reaction intensifies. Calculations were performed at the moment corresponding to half of the reaction time ($\alpha_r = 0.5$). The results are presented in **Table 1**.

Table 1. Experimental and calculated heat transfer data for a single stationary spherical FS90Ba4 alloy particle interacting with 13.3 % NaOH solution

Temperature of the solution in the reactor, t_m, °C	Temperature at the reaction surface, °C	Mean logarithmic temperature difference, °C	Pressure in the reactor, MPa	Pressure on the reacting surface, MPa	Half a reaction time, τ, s (α_r = 0,5)	Hydrogen evolution rate, $W_r \cdot 10^3$, m³/s	Radious of sphere of equivalent volume, $R_r \cdot 10^3$, m	Hydrogen evolution rate, $W_r \cdot 10^3$, m³/(m²·s)	Diameter of lifting flow, $d_{l.f.} \cdot 10^3$, m	Liquid flow velocity, m/s
98	181	21.7	0.42	0.77	1440	1.9	5.64	0.18	16.95	2.2
100	192	23.5	0.44	0.81	1470	2.1	5.61	0.2	16.74	2.1
128	238	26.9	0.68	1.28	390	2.4	5.49	13.4	16.14	2.26
130	251	29	0.76	1.47	450	9.2	5.37	13.8	16.43	2.18
137	265	30.3	0.84	1.61	630	9.7	5.26	17.1	16.66	2.12

The main kinetic studies were carried out in a hydrogen reactor operating under isochoric conditions (reactor internal volume, $V = 1.13 \times 10^{-3}$ m³). Hydrogen evolution proceeded without the addition of reactants or removal of reaction products. Experimental data on the interaction of spherical FS90Ba4 alloy samples with aqueous sodium hydroxide solution are presented in **Table 2** and **Figures 2** and **3**. The diameter of the FS90Ba4 alloy particles was $d = 1 \times 10^{-3}$ m.

Table 2. Dependence of the hydrogen evolution rate on temperature during the reaction of FS90Ba4 alloy with 13.3 % NaOH solution (hydrogen reactor, $V = 1.13 \times 10^{-3}$ m³)

№ Experiment	Initial solution temperature, t_0, °C	Maximum alloy temperature, t_{max}, °C	Time to reach maximum temperature, $\tau \cdot 10^{-3}$,	Maximum pressure, P_{max}, MPa	Time to reach the maximum pressure,, $\tau \cdot 10^{-3}$, sec	Total reaction time, $\tau \cdot 10^{-3}$, sec	Alloy mass, $m \cdot 10^3$, kg	Maximum hydrogen evolution rate, $W_{max} \cdot 10^3$, m³/(kg·s)
1	90[1)]	100	0.54	0,44	2.94	2.94	5	0.18
2	120[1)]	128	0.16	0.68	0.72	0.9	5	0.68
3	90	103	0.51	0.48	3	3	5	0.22
4	130	137	0.2	0.84	2.1	2.2	5	1.08
5	120	130	0.18	0.8	2.4	2.6	5	1.04

1) 10 % NaOH.

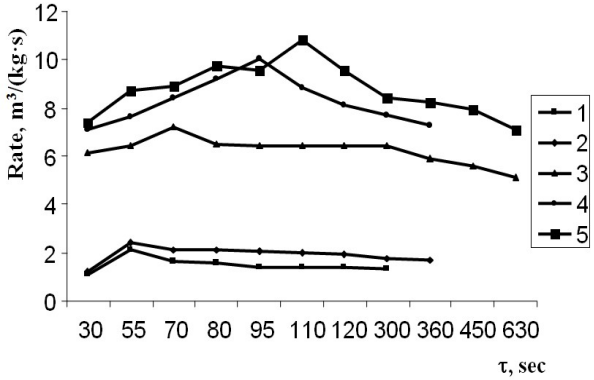

Figure 2. Time dependence of the hydrogen evolution rate for FS90Ba4 alloy reacting with aqueous sodium hydroxide solution (hydrogen reactor) at different initial temperatures: 1 – 100 °C (10 % NaOH); 2 – 103 °C (13.3 % NaOH); 3 – 128 °C (10 % NaOH); 4 – 130 °C (13.3 % NaOH); 5 – 137 °C (13.3 % NaOH).

The hydrogen evolution rate was calculated using the following equation

$$W = \frac{\Delta V}{m \cdot \Delta \tau},$$

where V is the volume of evolved hydrogen reduced to standard conditions, m³; $\Delta\tau$ is the time required for the evolution of this gas volume, s; m is the mass of the alloy, kg.

The flow rate of the generated hydrogen was measured using a GSB-400 flow meter. The pressure in the reactor does not exceed

0.93 MPa. The maximum hydrogen evolution rate under these conditions was

$W_{max} = 1.08\times10^{-3}$ m³/(kg·s) or $W'_{max} = 0.35\times10^{-3}$ m³/(m²·s) (**Table 2**).

A decrease in the temperature of the reaction medium in the reactor by 8-10 °C is observed upon falling of the cassette containing the FS90Ba4 alloy (particle size $d = 1\times10^{-3}$ m) into the sodium hydroxide solution. The induction period under these conditions is 3-5 seconds. A rapid temperature increase of 15-17 °C leads to a sharp acceleration of the reaction rate. The temperature spike lasts for 10-12 seconds (**Figure 3**).

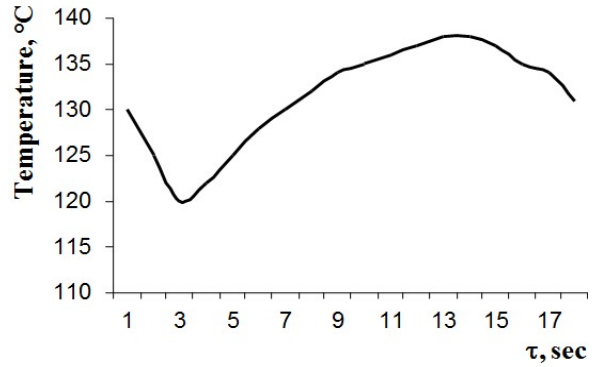

Figure 3. Temperature–time dependence for the reaction of FS90Ba4 alloy with 13.3 % NaOH solution (hydrogen reactor), t_{start} = 130 °C.

At the initial stage of the reaction, the temperature increases sharply. Subsequently, the rate of temperature rise slows down, which is explained by the influence of the forming FS oxide layer. After the temperature spike, the instrument indicates a gradual decrease in temperature, indicating the completion of the reaction due to the complete destruction of the alloy particles. In experiment № 4, at the final stage of the reaction, the temperature increased from 130 °C to 137 °C within 6 seconds (**Table 2**). Considering the short-lived nature of the reactive layer and the system's inertia, the actual temperature is estimated to reach 266 °C. Thus, the actual temperature rise is estimated to be 134 °C.

Recalculation for half of the reaction period (7.5 s) indicates a temperature increase from 100 °C to 194 °C, corresponding to a 94 °C spike. The value of 194 °C corresponds to the saturation temperature at the critical pressure, which corresponds to $\alpha_r = 0.5$. Increasing the initial reaction temperature for the FS90Ba4 alloy from 90 °C to 130 °C leads to a fivefold increase in the hydrogen evolution rate (**Table 2**, **Figure 3**).

After the temperature spike subsides, a gradual decrease in the reaction temperature is observed, indicating that the reaction has come to an end due to the complete destruction of the reacting alloy particles.

The actual flow-drainage velocity v^* was determined using the formula

$$v^* = \varphi \cdot v,$$

where $\varphi = 0.84$ is the phase sliding coefficient (it is determined by the method described in the article [13, 15]); v – velocity of the fluid flow around the particles, m/s.

The particle velocity is determined by the following equation

$$\frac{U}{v} = 0.72 \cdot \left[\frac{v^2}{g \cdot D}\frac{(\rho-\rho_0)}{\rho_0}\right]^{0.14},$$

where U is velocity of the moving particle, m/s; v is velocity of the moving fluid, m/s; g is free fall acceleration, m/s²; D = 0.072 m – diameter of the hydrogen reactor ($V = 1.13\times10^{-3}$ m³); ρ, ρ_0 are the densities of the solid phase and transported flow, kg/m³.

The experimental and calculated data on the interaction of spherical samples of FS90Ba4 and AG5O5In5 alloys with an aqueous NaOH solution and water in a hydrogen reactor are presented in **Table 3**.

Table 3. Experimental and calculated data on the interaction of spherical samples of FS90Ba4 and AG5O5In5 alloys with an aqueous NaOH solution and H_2O in a hydrogen reactor ($V = 1.13\times10^{-3}$ m³)

Alloys	Reaction solution	Temperature of the reaction solution, °C	Pressure in the reactor, MPa	Half a reaction time, τ, s ($\alpha_r = 0,5$)	Hydrogen evolution rate, $W_\tau \cdot 10^3$, m³/s	Liquid flow velocity, m/s
FS90Ba4	13.3 % NaOH	100 130 137	0.55 0.7 0.74	1500 1200 980	2.85 3.5 9.7	2.19 2.3 2.32
AG5O5In5 [37]	H_2O	90 78 76	0.46 0.54 0.38	300 330 480	7.14 6.6 4.56	2.3 2.1 1.99

The velocities of motion and fluid flow velocity around of spherical FS90Ba4 alloy particles at a temperature of 100 °C are U = 1.68 m/s and ν = 2.19 m/s, respectively. The experiments were conducted in a reactor with a volume of $V = 1.13\times10^{-3}$ m³. For spherical AG5O5In5 alloy particles at a temperature of 90 °C, U = 1.81 m/s and ν = 2.3 m/s, while the maximum rate of hydrogen evolution from water is $W = 7.14\times10^{-3}$ m³/(m²·s) [37], which is more than twice the hydrogen evolution rate for the ferrosilicon alloy.

Determination of the reaction temperature range, particle motion velocities, and fluid flow around ferrosilicon and aluminum alloy particles enables the calculation of the main heat and mass transfer parameters and refinement of the methodology for designing hydrogen generators using silicon- and aluminum-based alloys. The use of ferrosilicon alloys with alkaline earth metal additives as an energy-storage material, compared with activated aluminum, makes it possible to reduce the cost of the hydrolytic hydrogen production process.

Conclusions:

The behavior of temperature changes during the interaction of a stationary ferrosilicon alloy sample ($m = 4.2\times10^{-3}$ kg) with an aqueous NaOH solution in a glass reactor at an initial reaction temperature of 95 °C was examined.

As the reaction front approaches the thermocouple junction located at the center of the sample, a sharp temperature increase of 7-9 °C is observed under boiling and gas evolution conditions. The temperature difference between the reaction solution and the center of the ferrosilicon alloy sample was in the range of 88-97 °C.

For the FS 90Ba4 alloy in the hydrogen reactor, increasing the initial reaction temperature from 90 °C to 130 °C led to a fivefold increase in the hydrogen evolution rate, accompanied by a sharp temperature rise of 15–17 °C during the initial stage of the reaction. This temperature spike persists for 10-12 seconds.

Determination of the reaction temperature range, particle motion velocities, and fluid flow around ferrosilicon and

aluminum alloy particles enables the calculation of the main heat and mass transfer parameters and refinement of the methodology for designing hydrogen generators using silicon- and aluminum-based alloys. The use of ferrosilicon alloys with alkaline earth metal additives as an energy-storage material, compared with activated aluminum, makes it possible to reduce the cost of the hydrolytic hydrogen production process.

References

[1] Wang R, Liu Y, Zuo P, Zhang Z, Lei N, Liu Y. Phthalocyanine-sensitized evolution of hydrogen and degradation of organic pollutants using polyoxometalate photocatalysts. Environmental Science and Pollution Research 2020;27(15):18831-18842.

[2] Vishwanath R, Kandaiah S. Facile electrochemical growth of nanostructured copper phthalocyanine thin film via simultaneous anodic oxidation of copper and dilithium phthalocyanine for photoelectrochemical hydrogen evolution. Journal of Solid State Electrochemistry 2015;20(3):767-773.

[3] Wu X, Dong C. Near-infrared-responsive gold nanoparticle-based photothermal agents. Photonanotechnology for Therapeutics and Imaging 2020:83-104.

[4] Yıldız B, Güzel E, Akyüz D, Arslan B, Koca A, Şener M. Unsymmetrically pyrazole-3-carboxylic acid substituted phthalocyanine-based photoanodes for use in water splitting photoelectrochemical and dye-sensitized solar cells. Solar Energy 2019;191:654-662.

[5] Takanabe K, Kamata K, Wang X, Antonietti M, Kubota J, Domen K. Photocatalytic hydrogen evolution on dye-sensitized mesoporous carbon nitride photocatalyst with magnesium phthalocyanine. Physical Chemistry Chemical Physics 2010;12(40):13020.

[6] Tedesco A, Primo F, Beltrame M. Phthalocyanines: Synthesis, Characterization and Biological Applications of Photodynamic Therapy (PDT), Nanobiotechnology, Magnetohyperthermia and Photodiagnosis (Theranostics). Reference Module in Materials Science and Materials Engineering 2016.

[7] Sudi M, Zhao L, Wang Q, Dou Y, Shen X, Wang A, Zhu W. Efficient photoelectrochemical water splitting of metal-porphyrin decorated on BiVO4 photoanode. Applied Surface Science 2022;606:154753.

[8] Nikolic V, Tasic G, Maksic A, Saponjic D, Miulovic S, Marceta Kaninski M. Raising efficiency of hydrogen generation from alkaline water electrolysis – Energy saving. International Journal of Hydrogen Energy 2010;35(22):12369-12373.

[9] Moradi Nafchi F, Afshari E, Baniasadi E, Javani N. A parametric study of polymer membrane electrolyser performance, energy and exergy analyses. International Journal of Hydrogen Energy 2019;44(34):18662-18670.

[10] Min G, Choi S, Hong J. A review of solid oxide steam-electrolysis cell systems: Thermodynamics and thermal integration. Applied Energy 2022;328:120145.

[11] Mabrak H, Elmazouzi S, Takky D, Naimi Y, Colak I. Hydrogen Production by Water Electrolysis: Review. 2023 12th International Conference on Renewable Energy Research and Applications (ICRERA) 2023:372-380.

[12] Kaplan B, Kırlıoğlu A, Alinezhadfar M, Zabara M, Mojarrad N, Iskandarani B, Yürüm A, Ozkan C, Ozkan M, Gürsel S. Hydrogen production via electrolysis: Operando monitoring and analyses. Chem Catalysis 2023;3(5):100601.

[13] Kim J, Jun A, Gwon O, Yoo S, Liu M, Shin J, Lim T, Kim G. Hybrid-solid oxide electrolysis cell: A new strategy for efficient hydrogen production. Nano Energy 2018;44:121-126.

[14] Mabrak H, Elmazouzi S, Takky D, Naimi Y, Colak I. Hydrogen Production by Water Electrolysis: Review. 2023 12th International Conference on Renewable Energy Research and Applications (ICRERA) 2023:372-380.

[15] Zhang F, Zhao P, Niu M, Maddy J. The survey of key technologies in hydrogen energy storage. International Journal of Hydrogen Energy 2016;41(33):14535-14552.

[16] Zipunnikov NN, Troshenkin VB, Troshenkin BA. Feasibility Study of Ferro-Silico- Aluminum Alloys Production and the Use for Hydrogen Generation from Water. Herald of NTU "KhPI". 2013;9(983):24-32.

[17] Soler L, Macanás J, Muñoz M, Casado J. Aluminum and aluminum alloys as sources of hydrogen for fuel cell applications. Journal of Power Sources 2007;169(1):144-149.

[18] Ancona M, Antonioni G, Branchini L, De Pascale A, Melino F, Orlandini V, Antonucci V, Ferraro M. Renewable Energy Storage System Based on a Power-to-Gas Conversion Process. Energy Procedia 2016;101:854-861.

[19] Kotowicz J, Bartela Ł, Węcel D, Klaudia D. Hydrogen generator characteristics for storage of renewably-generated energy. Energy 2016;118:156-171.

[20] Czech E, Troczynski T. Hydrogen generation through massive corrosion of deformed aluminum in water. International Journal of Hydrogen Energy 2010;35(3):1029-1037.

[21] Soler L, Macanás J, Muñoz M, Casado J. Synergistic hydrogen generation from aluminum, aluminum alloys and sodium borohydride in aqueous solutions. International Journal of Hydrogen Energy 2007;32(18):4702-4710.

[22] Flores-Chan J, Bedolla-Jacuinde A, Patiño-Carachure C, Rosas G, Espinosa-Medina M. Corrosion study of Al–Fe (20 wt-%) alloy in artificial sea water with NaOH additions. Canadian Metallurgical Quarterly 2017;57(2):201-209.

[23] Yang B, Zhu J, Jiang T, Gou Y, Hou X, Pan B. Effect of heat treatment on Al Mg Ga In Sn alloy for hydrogen generation through hydrolysis reaction. International Journal of Hydrogen Energy 2017;42(38):24393-24403.

[24] Troshenkin VB, Zippunikov NN. State of developments on the study of the process and design of equipment for the production of hydrogen from water using alloys. Herald of NTU "KhPI". 2008;12:51-55.

[25] Troshenkin BA, Troshenkin VB. Nucleation at boiling and condensation. Modern science: research, ideas, results, technologies 2011;1:242-246.

[26] Zipunnikov M, Bukhkalo S, Kotenko A. Researching The Process Of Hydrogen Generating From Water With The Use Of The Silicon Basis Alloys. French-Ukrainian Journal of Chemistry 2019;7(2):138-144.

[27] Solovey VV, Zipunnikov MM, Poda VB, Vorobjova IO. Hydrogen generation from water by using alloys based on silicon and aluminium. Voprosy Khimii i Khimicheskoi Tekhnologii 2020;(4):148-156.

[28] Chen X, Zhao Z, Hao M, Wang D. Research of hydrogen generation by the reaction of Al-based materials with water. Journal of Power Sources 2013;222:188-195.

[29] Troshen'kin V. Characteristic features of calculations of hydrogen generators. Journal of Engineering Physics and Thermophysics 2010;83(1):165-170.

[30] Berezovets V, Kytsya A, Zavaliy I, Yartys V. Kinetics and mechanism of MgH2 hydrolysis in MgCl2 solutions. International Journal of Hydrogen Energy 2021;46(80):40278-40293.

[31] Verbovytskyy Y, Berezovets V, Kytsya A, Zavaliy I, Yartys V. Hydrogen Generation by the Hydrolysis of MgH2. Materials Science 2020;56(1):1-14.

[32] Kytsya A, Berezovets V, Verbovytskyy Y, Bazylyak L, Kordan V, Zavaliy I, Yartys V. Bimetallic Ni-Co nanoparticles as an efficient catalyst of hydrogen generation via hydrolysis of NaBH4. Journal of Alloys and Compounds 2022;908:164484.

[33] Tegel M, Schöne S, Kieback B, Röntzsch L. An efficient hydrolysis of MgH2-based materials. International Journal of Hydrogen Energy 2017;42(4):2167-2176.

[34] Hiraki T, Hiroi S, Akashi T, Okinaka N, Akiyama T. Chemical equilibrium analysis for hydrolysis of magnesium hydride to generate hydrogen. International Journal of Hydrogen Energy 2012;37(17):12114-12119.

[35] Brack P, Dann S, Wijayantha K, Adcock P, Foster S. Synthesis of activated ferrosilicon-based microcomposites by ball milling and their hydrogen generation properties. International Journal of Hydrogen Energy 2019;44(35):19113-19127.

[36] Santos P, Santos H, Toledo S. Standard transition aluminas. Electron microscopy studies. Materials Research 2000;3(4):104-114.

[37] Troshenkin VB. Heat and mass transfer during the interaction of activated aluminum with water. Herald of Kharkiv Polytechnic University 1999;49:14-18.